

Cyclic Peptide–Selenium Nanoparticles as Drug Transporters

Amir Nasrolahi Shirazi,^{†,‡,§} Rakesh K. Tiwari,^{†,‡,§} Donghoon Oh,[§] Brian Sullivan,[§] Anil Kumar,[§] Yousef A. Beni,^{§,||} and Keykavous Parang*,^{†,‡,§}

[†]Chao Family Comprehensive Cancer Center, School of Medicine, University of California, Irvine, Shanbrom Hall, 101 The City Drive South, Orange, California 92868, United States

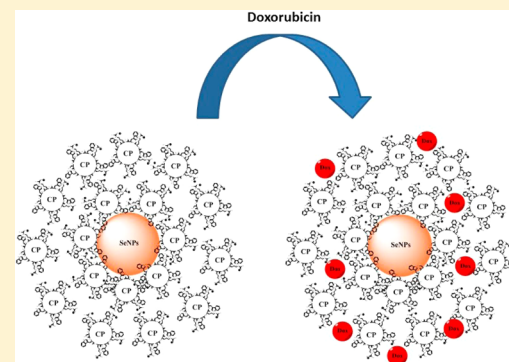
[‡]Chapman University School of Pharmacy, Harry and Diane Rinker Health Science Campus, Irvine, California 92618, United States

[§]Department of Biomedical and Pharmaceutical Sciences, College of Pharmacy, University of Rhode Island, Kingston, Rhode Island 02881, United States

Supporting Information

ABSTRACT: A cyclic peptide composed of five tryptophan, four arginine, and one cysteine [W_5R_4C] was synthesized. The peptide was evaluated for generating cyclic peptide-capped selenium nanoparticles (CP–SeNPs) *in situ*. A physical mixing of the cyclic peptide with SeO_3^{2-} solution in water generated [W_5R_4C]-SeNPs via the combination of reducing and capping properties of amino acids in the peptide structure. Transmission electron microscopy (TEM) images showed that [W_5R_4C]-SeNPs were in the size range of 110–150 nm. Flow cytometry data revealed that a fluorescence-labeled phosphopeptide (F'-PEpYLGLD, where F' = fluorescein) and an anticancer drug (F'-dasatinib) exhibited approximately 25- and 9-times higher cellular uptake in the presence of [W_5R_4C]-SeNPs than those of F'-PEpYLGLD and dasatinib alone in human leukemia (CCRF-CEM) cells after 2 h of incubation, respectively. Confocal microscopy also exhibited higher cellular delivery of F'-PEpYLGLD and F'-dasatinib in the presence of [W_5R_4C]-SeNPs compared to the parent fluorescence-labeled drug alone in human ovarian adenocarcinoma (SK-OV-3) cells after 2 h of incubation at 37 °C. The antiproliferative activities of several anticancer drugs doxorubicin, gemcitabine, clofarabine, etoposide, camptothecin, irinotecan, epirubicin, fludarabine, dasatinib, and paclitaxel were improved in the presence of [W_5R_4C]-SeNPs (50 μM) by 38%, 49%, 36%, 36%, 31%, 30%, 30%, 28%, 24%, and 17%, respectively, after 48 h incubation in SK-OV-3 cells. The results indicate that CP–SeNPs can be potentially used as nanosized delivery tools for negatively charged biomolecules and anticancer drugs.

KEYWORDS: antiproliferative, drug delivery, metal, nanoparticle, selenium



■ INTRODUCTION

Efficient delivery of drugs to their targets can significantly improve their therapeutic potency. Drug delivery systems (DDSs) have been introduced as novel tools to improve the pharmacodynamics and pharmacokinetics properties of drugs. To increase the stability, bioavailability, and intracellular uptake and to reduce the toxicity, a wide range of DDSs were constructed recently from different materials including polymers, peptides, and liposomes.¹ The potential applications of nanotechnology in developing new DDSs have been investigated.^{2,3}

Nanodrug delivery systems (nano-DDSs) have offered several advantages compared to larger DDSs, such as lower toxicity and improved cellular uptake. The highly active surface area of nanoparticles provides maximized loading capacity of cargo molecules. Furthermore, when small sized nanoparticles get functionalized properly, they can go through rapid dissolution and enhanced adhesion to the biological target surfaces providing great bioavailability at the site of the action.⁴

Nano-DDS containing metal nanoparticles (metal nano-DDSs) have emerged as effective tools for the treatment of

various diseases.⁵ Metal nano-DDSs containing hydrophobic and hydrophilic segments have been investigated for carrier-mediated drug delivery through entrapping hydrophobic and hydrophilic cargo molecules because of their amphiphilic properties. Moreover, metal nano-DDS has become a subject of major attention because of their nonimmunogenicity and biocompatibility.⁶

Among various metal nanoparticles, selenium nanoparticles (SeNPs) have not been investigated extensively. Selenium (Se) is an essential micronutrient with a recommended dietary intake of 55 μg/day.⁷ Although selenium is required for normal cellular function, high doses of selenium in the form of SeNPs could selectively kill malignant cells.⁸ Thus, there is a compelling need to design novel SeNPs that could be used as nontoxic nano-DDSs.

Received: May 16, 2014

Revised: August 3, 2014

Accepted: September 3, 2014

Published: September 3, 2014



Two parameters including the chemical entity of selenium and the concentration are responsible for its toxicity and anticancer activity. Selenium can be found in different oxidation states, i.e., selenite (SeO_3^{2-}) oxyanions, selenite (SeO_4^{2-}), and elemental selenium (Se^0) where the oxidation states are +4, +6, and 0, respectively. It has been previously reported that changing the redox state of the metal ions can reduce or eliminate their toxicity.⁶

SeNPs have been coated or functionalized with other compounds to improve their biological profile. Previous studies have shown that bovine serum albumin coated with SeNPs (BSA–SeNPs) exhibit similar activity to selenomethionine (SeM) and Se-methylselenocysteine (SeMSC) in increasing the activity of selenoenzymes and Se levels in tissue, and showed less toxicity than organic Se compounds. Thus, the dose and chemical form of Se have become critical to reduce the toxicity and to increase the therapeutic effects.⁹ Furthermore, the size of nanoparticles is a critical element that can alter their biological properties.^{10,11}

Recently, Liu and co-workers developed a facile procedure for the preparation of 5-fluorouracil surface-decorated SeNPs with improved anticancer activity. It was found that the surface functionalization of spherical SeNPs with 5-fluorouracil through physical adsorption increased the uptake of the SeNPs by cells.¹² Furthermore, to improve the cellular uptake of SeNPs, their surface has been decorated by various ligands, such as ATP,¹³ Spirulina polysaccharide,¹⁶ mushroom polysaccharides-protein,¹⁵ and chitosan.¹⁴ Although these methods disclosed new aspects of SeNPs application, they suffer from multistep synthesis, purifications, and inherent toxicity of nano-DDSs. Furthermore, the majority of carriers were found to be energy-dependent since they use endocytic pathways to cross the membrane. Thus, there is a need to develop new biomaterials for the functionalization of the surface of SeNPs.

Peptides are commonly used as nanoscaled systems for carrier-mediated drug delivery because of their ability to carry a wide range of cargo molecules through encapsulation. Moreover, peptides have been used as a component in the structure of nano-DDSs by taking advantage of a broad range of amino acids with different physicochemical properties. For example, peptide-functionalized gold nanoparticles have been employed as one of the prior biocompatible systems in drug delivery^{17–20} and improved the cellular delivery of several drugs via noncovalent complexation significantly.²¹

The design and synthesis of homochiral L-cyclic peptides and their application for the nuclear targeting delivery of anti-HIV drugs and biomolecules have been reported by us.²² Moreover, physical mixing of the cyclic peptide containing arginine, tryptophan, and HAuCl₄ resulted in the generation of peptide-capped gold nanoparticles and increased the cellular delivery of drugs and biomolecules dramatically.^{23,24}

We report here synthesis and evaluation of a cyclic cell-penetrating peptide composed of ten amino acids including arginine, tryptophan, and cysteine. Cysteine was selected to improve binding to Se through S–Se bond formation. The ability of the peptide for in situ synthesis of cyclic peptide-capped selenium nanoparticles (CP–SeNPs) was investigated. Subsequently, CP–SeNPs were evaluated as a nanometal DDS for the delivery of a model anticancer drug, dasatinib, and a negatively charged cell-impermeable phosphopeptide. Furthermore, CP–SeNPs were used to improve the antiproliferative activity of a number of anticancer agents. This work is distinct from the previous work since the double-barreled novel delivery

system that includes cyclic peptides and SeNPs significantly improves the antiproliferative activity of anticancer agents.

EXPERIMENTAL SECTION

General. Materials. Peptide synthesis reagents, including coupling reagents, H-Arg(Pbf)-2-chlorotriptyl resin, and Fmoc-amino acids, were purchased from Chempep (Miami, FL). The other reagents were obtained from Sigma-Aldrich Chemical Co. (Milwaukee, WI). The cell lines were purchased from American Type Culture Collection (ATCC).

Methods. The cyclic peptide [$\text{W}_5\text{R}_4\text{C}$] was synthesized based on our previously reported methodology.^{25,26} The synthesis was performed in QUARK glass vessels by mixing through bubbling nitrogen gas into the mixture at room temperature unless otherwise mentioned. Fmoc/tBu solid phase procedure was used for the synthesis of the peptide. The coupling and activating reagents were 2-(1H-benzotriazole-1-yl)-1,1,3,3-tetramethyluronium hexafluorophosphate (HBTU) and *N,N*-diisopropylethylamine (DIPEA), respectively, in anhydrous *N,N*-dimethylformamide (DMF). The Fmoc group was deprotected using piperidine in DMF (20% v/v).

The H-Arg(Pbf)-2-chlorotriptyl resin (730 mg, 0.3 mmol, 0.41 mmol/g) was added to QUARK glass vessels followed by the addition of DMF (50 mL) and mixing through bubbling nitrogen gas into the mixture for 30 min. This procedure was repeated two more times. The solvent was drained followed by coupling of Fmoc-Trp(Boc)-OH (473.9 mg, 0.9 mmol) using HBTU (341.6 mg, 0.9 mmol) and DIPEA (313.4 μ L, 1.8 mmol) in anhydrous DMF (10 mL) for 1.5 h. The resin was washed using DMF (15 mL \times 3) followed by deprotection of Fmoc group with 20% piperidine in DMF. The resin was washed with DMF (15 mL \times 3) and coupled with Fmoc-Arg(Pbf)-OH (583.9 mg, 0.9 mmol) and followed by deprotection of the Fmoc group. The coupling and deprotection cycles were repeated to complete the synthesis of protected peptide sequence on resin. The last coupling was performed with Fmoc-Cys(Trt)-OH (583.9 mg, 0.9 mmol) followed by deprotection of Fmoc group and washing the resin. The protected peptide was cleaved from the resin by agitating the resin with a cleavage cocktail of trifluoroethanol (TFE)/acetic acid/DCM (2:2:6 v/v/v, 15 mL) for 2 h. The resin was filtered off, and the cleavage cocktail was removed using a rotatory evaporator to provide solid linear protected peptide for cyclization. The solid linear protected peptide was dissolved in DMF/DCM (150 mL, 2:1 v/v) under nitrogen atmosphere followed by the addition of coupling reagents *N,N*-diisopropylcarbodiimide (DIC, 93.5 μ L, 0.6 mmol) and 1-hydroxy-7-azabenzotriazole (HOAt, 81.6 mg, 0.6 mmol). The mixture was stirred for 12 h at room temperature. The solvent was removed using a rotary evaporator. The cleavage of side chain protecting group was conducted by using cleavage cocktail trifluoroacetic acid (TFA)/thioanisole/anisole/ethanedithiol (EDT) (10 mL, 90:5:2:3 v/v/v/v) for 2 h. The crude peptide was precipitated with diethyl ether followed by centrifugation to provide solid crude cyclized peptide. The crude peptide was purified using reverse phase chromatography using a Hitachi LaChrom Elite reversed-phase high-performance liquid chromatograph (RP-HPLC) on a Phenomenex Gemini Axia packed C18 (250 \times 21.2 mm, 10 μ m) and using flow rate of 10 mL/min with a gradient system of 0–100% acetonitrile (0.1% TFA) and water (0.1% TFA) over 60 min to elute the pure fraction. Evaporation and lyophilization afforded

pure powdered cyclic peptide. The purity of the final product ($\geq 95\%$) was confirmed by analytical RP-HPLC that was carried out on Hitachi analytical HPLC system using a Shimadzu Premier C18 column (150×4.6 mm, $3 \mu\text{m}$) and with a gradient system ($\text{H}_2\text{O}/\text{CH}_3\text{CN}$) at a flow rate of 1 mL/min and 220 nm . The peptide structure was confirmed by high-resolution matrix-assisted laser desorption–ionization time-of-flight (MALDI TOF/TOF) mass spectrometer (Shimadzu Biotech). MALDI-TOF (m/z) [$\text{C}_{82}\text{H}_{103}\text{N}_{27}\text{O}_{10}\text{S}$]: calcd, 1657.8080; found, 1658.7102; [$\text{M} + \text{H}]^+$, 1680.4571 [$\text{M} + \text{Na}]^+$, 1696.7428 [$\text{M} + \text{K}]^+$.

Preparation of Cyclic $[\text{W}_5\text{R}_4\text{C}]$ -SeNPs. The synthesis of SeNPs was carried out by reacting the selenium solution with the cyclic peptide. The stock solution of the peptide (10 mM) was mixed with Na_2SeO_3 solution in water (10 mM) at 50°C . The reaction mixture color became orange indicating the formation of peptide capped–SeNPs after 6 h. This experiment was repeated for more than 10 times. After the formation of $[\text{W}_5\text{R}_4\text{C}]$ -SeNPs, the stock solution was diluted into desired concentration for further experiments.

Synthesis of Fluorescence-Labeled Dasatinib (F' -Das). To synthesize the fluorescence-labeled dasatinib (F' -Das), the drug was conjugated through using a glycine linker as elaborated in the Supporting Information (Scheme S1), where F' = fluorescein.

Transmission Electron Microscopy (TEM). TEM sample was prepared by using an aqueous solution of $[\text{W}_5\text{R}_4\text{C}]$ -SeNPs ($5 \mu\text{L}$ of 5 mM) according to our previously reported procedure and analyzed.²³

To load $[\text{W}_5\text{R}_4\text{C}]$ -SeNPs by doxorubicin (Dox), an aqueous solution of $[\text{W}_5\text{R}_4\text{C}]$ -SeNPs (5 mM) and Dox ($500 \mu\text{M}$) were mixed in water to end up with 10:1 ratio. The solution was vortexed at room temperature for 5 min. Similar sample preparation method for TEM imaging was employed as explained above.

Circular Dichroism. CD studies were conducted according to our previously reported method.⁴⁰ All experiments on the samples including $[\text{W}_5\text{R}_4\text{C}]$ ($50 \mu\text{M}$, H_2O), $[\text{W}_5\text{R}_4\text{C}]$ -SeNPs ($50 \mu\text{M}$, H_2O), and camptothecin (CPT, $5 \mu\text{M}$, DMSO) were performed by using a ratio of 10:1 between the carrier and the drug at room temperature. All measurements were performed in triplicate.

Cell Culture and Cytotoxicity Assay. Cell Culture. Ovarian adenocarcinoma (SK-OV-3, ATCC no HTB-77), human leukemia (CCRF-CEM, ATCC no. CCL-119), and human embryonic kidney epithelial (HEK-293T, ATCC no. CRL-11268) cells were purchased from ATCC. Cell culture flasks (75 cm^2) were used for culturing cells. Two different media were used. RPMI-16 medium was used for CCRF-CEM cells, and EMEM medium was used for SK-OV-3 and HEK-293T cells, containing fetal bovine serum (FBS, 10%), and the penicillin–streptomycin solution (1%, 10 000 units of penicillin and streptomycin (10 mg in 0.9% NaCl)) in a humidified atmosphere of CO_2 (5%) and air (95%) at 37°C .

Cytotoxicity Assay of $[\text{W}_5\text{R}_4\text{C}]$ -SeNPs. The cytotoxicity assay was performed by using SK-OV-3 (5000), HEK-293T (4000), and CCRF-CEM (40 000) cells based on our reported procedure.⁴⁰ The only modification was that the old medium was not replaced in the case of CCRF-CEM by treatments. The compounds were added to the old medium instead. All assays were conducted in triplicate assays.

Antiproliferative Activity Assay in Time-Dependent Studies. Antiproliferative activities of several anticancer drugs

including Dox, irinotecan, gemcitabine, epirubicin, dasatinib, etoposide, paclitaxel, camptothecin, fludarabine, and clofarabine were evaluated in SK-OV-3 with $[\text{W}_5\text{R}_4\text{C}]$ -SeNPs, and the results were compared with those of drugs alone after 48 h. The antiproliferative assay was performed by employing our previously reported method and reagents.^{24,26} DMSO (1% in water) was used as a control. Furthermore, the entrapment of the drugs was also carried out by using our previously reported procedure.⁴² All assays were conducted in triplicate assays.

Flow Cytometry. Six-well plates with opti-MEM were used for seeding CCRF-CEM cells (1×10^7). In the next step, the fluorescence-labeled dasatinib (F' -dasatinib) or F' -PEpYGLD ($5 \mu\text{M}$) was added to each well containing $[\text{W}_5\text{R}_4\text{C}]$ ($50 \mu\text{M}$) and $[\text{W}_5\text{R}_4\text{C}]$ -SeNPs ($50 \mu\text{M}$) in opti-MEM. The plates were incubated for 2 h at 37°C . The rest of the assay was performed under a similar condition as described earlier.^{24,26} All assays were conducted in triplicate assays.

Confocal Microscopy on Live Cells. SK-OV-3 cells were grown on coverslips in 6-well plates (1×10^5 cells per well) overnight. The fluorescence-labeled treatments with either F' -dasatinib or F' -PEpYGLD ($5 \mu\text{M}$) in the presence and absence of $[\text{W}_5\text{R}_4\text{C}]$ -SeNPs ($50 \mu\text{M}$) were added to cells in opti-MEM for 2 h at 37°C . The procedures for washing the slides and staining the cell nuclei by 4,6-diamidino-2-phenylindole (DAPI) were previously reported by us.⁴⁰ All assays were conducted in triplicate assays.

Drug Loading. Dox solution ($100 \mu\text{L}$ of $200 \mu\text{M}$) was mixed with $[\text{W}_5\text{R}_4\text{C}]$ -SeNPs solution in water ($400 \mu\text{L}$ of $500 \mu\text{M}$). The concentration ratio of Dox and peptide-capped SeNPs was maintained to be 1:10. A dialysis membrane (1 mL and molecular weight cutoff of 1000 D; Float-A-Lyzer G2, Spectrum Laboratories) was used for nanoparticle-loaded Dox. The methods for HPLC and quantifying the Dox amount was previously reported by us.⁴⁰ All measurements were performed in triplicate.

To calculate the loading efficiency, the following equation was used:

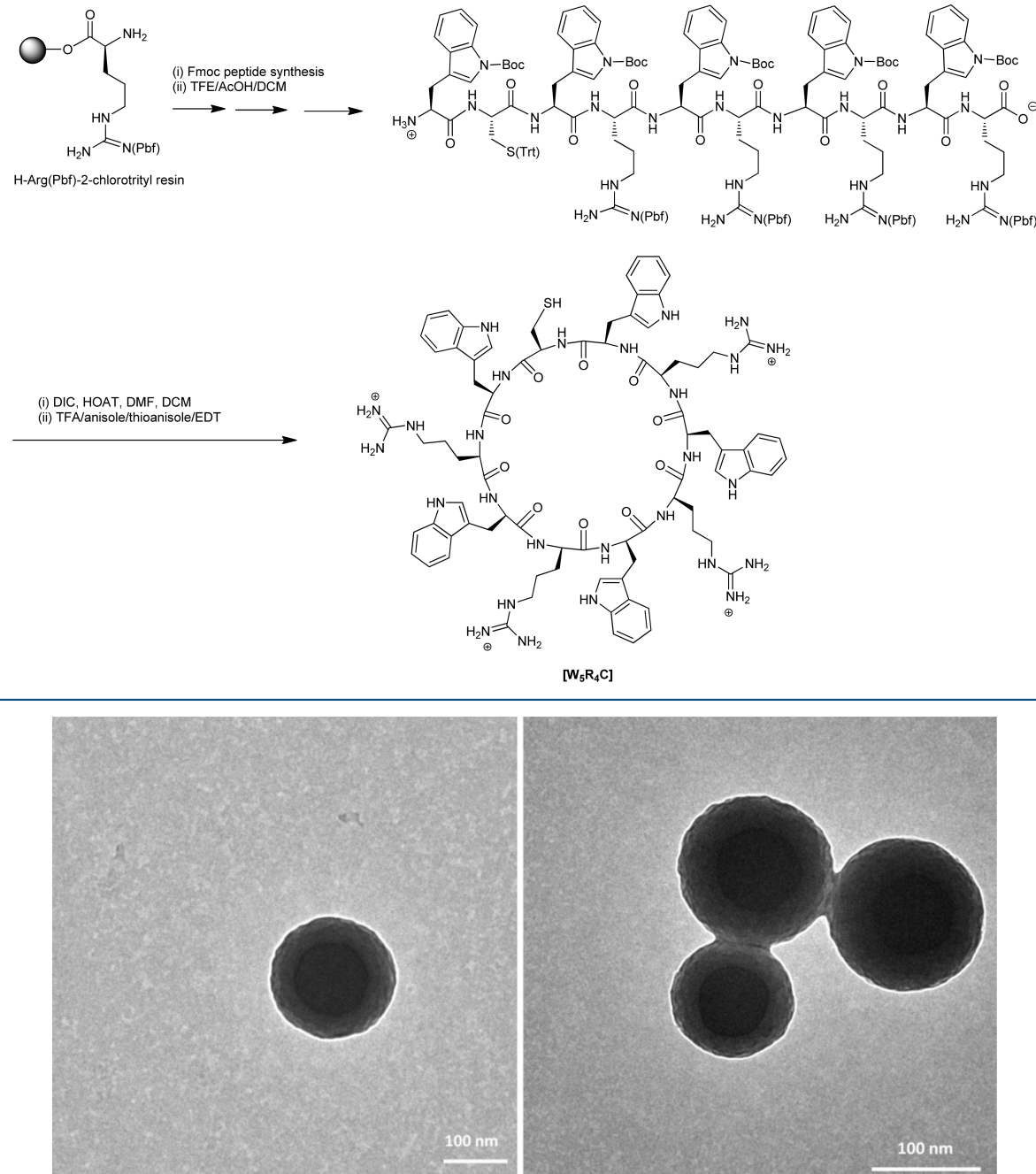
$$\begin{aligned} \text{loading efficiency(wt/wt, \%)} \\ = \frac{\text{Dox in feed} - \text{free Dox}}{\text{Dox in feed}} \times 100 \end{aligned}$$

To calculate the loading capacity, the quantity of SeNPs in the dialysis membrane was analyzed by using inductively coupled plasma mass spectrometry (ICP–MS) after 24 h. The ICP–MS results exhibited that $2.94 \mu\text{g}$ of SeNPs were accountable for Dox encapsulation. The loading capacity equation was used for the calculation as shown below:

$$\begin{aligned} \text{loading capacity(wt/wt, \%)} \\ = \frac{\text{Dox in feed} - \text{free Dox}}{\text{peptide capped with SeNPs in feed}} \times 100 \end{aligned}$$

Cellular Release. Dox intracellular release was investigated by using an HPLC technique as described previously.⁴⁰ At the beginning, the cells were seeded into 6-well plates (1×10^7 in 2 mL of medium per well). The Dox-loaded $[\text{W}_5\text{R}_4\text{C}]$ -SeNPs ($5:50 \mu\text{M}$) was added to cells in medium. The cells were incubated for 2–48 h at 37°C . The remaining of the procedure was similar as described by us.⁴⁰ All measurements were performed in triplicate.

Encapsulation of Camptothecin (CPT). Camptothecin solution (DMSO, $10 \mu\text{L}$ of 10^{-3} M) was mixed with the

Scheme 1. Chemical Structure of the Cyclic Peptide**Figure 1.** TEM images of $[W_5R_4C]$ -SeNPs.

peptide-capped SeNPs solution in water ($100 \mu\text{L}$ of 10^{-4} M) to adjust the molar ratio to be 1:1. A solution of CPT in DMSO was used as a negative control. The remaining of the procedure was conducted as previously reported by us.⁴⁰ All measurements were performed in triplicate.

RESULTS AND DISCUSSION

Chemistry. The cyclic decapeptide $[W_5R_4C]$ was synthesized by employing Fmoc/tBu-based solid phase chemistry (Scheme 1) as described previously.^{22–26} In brief, the linear protected peptide was first synthesized, followed by cleavage of side chain-protected peptide from the resin and cyclization in dilute conditions using DIC/HOAt in DMF/DCM solution for

12 h. After cyclization, the side chain of protected peptide was deprotected by using cleavage cocktail followed by reverse phase HPLC purification to afford pure cyclic peptide.

Evaluation of $[W_5R_4C]$ for Generating Peptide-SeNPs and Characterization. The synthesized $[W_5R_4C]$ was examined for its ability to generate SeNPs. The reaction was carried out via physical mixing of the peptide solution (10 mM) with the solution of Na_2SeO_4 (10 mM) in water at 50°C . The solution was colorless at the beginning of the reaction. However, after 6 h of incubation at 50°C , the color was turned to orange showing the formation of SeNPs.

This strategy is a one-pot reaction without any surface functionalization of SeNPs. Mechanistically, $[W_5R_4C]$ works as

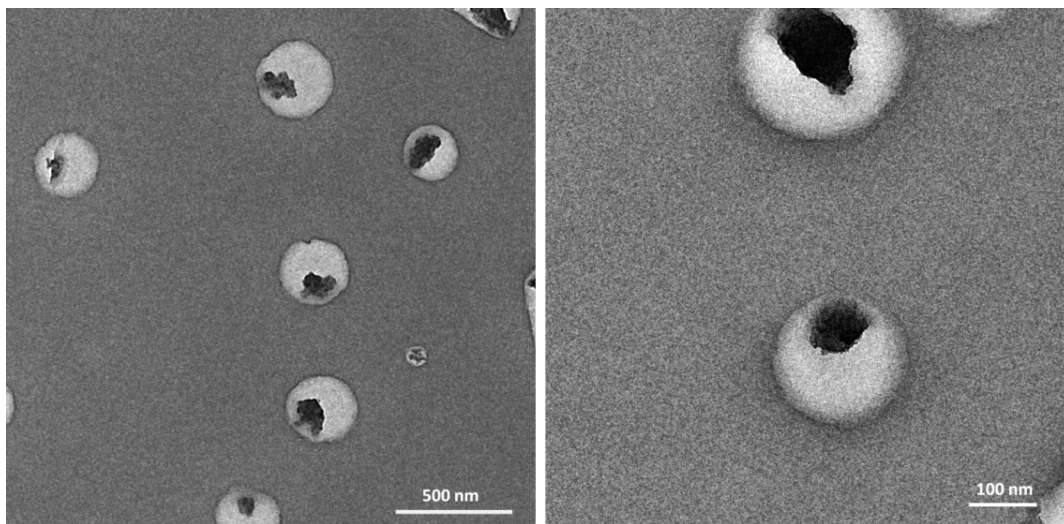


Figure 2. TEM images of $[W_5R_4C]$ -SeNP-loaded Dox.

reducing and capping agents. Tryptophan (W) is known to have the most efficient reducing capability compared to the other 19 amino acids.²⁷ Positively charged arginine (R) residues enhanced the reducing activity of the peptide via the appropriate ionic interactions with the negatively charged selenite anions.²³ Cysteine facilitated the formation of SeNPs possibly through stabilizing the formed nanoparticles by favorable S–Se bond formation.

Transmission Electron Microscopy (TEM). To investigate the morphology and size of $[W_5R_4C]$ -SeNPs, further studies were conducted using TEM. TEM images exhibited that $[W_5R_4C]$ -SeNPs formed spherical nanostructures with a size in the range of 110–150 nm after 1 day of incubation of the sample (Figure 1). The images revealed that the SeNPs were surrounded with a layer of peptide. We assume the presence of some noncovalent and/or covalent interactions between SeNPs and peptide as binding ligands.

Positively charged arginines and hydrophobic tryptophans contribute to intermolecular interactions and this morphology. The induced hydrophobic interactions by tryptophan residues possibly lead to the formation of peptide-coated SeNPs. Moreover, cysteine is probably involved in the formation of this morphology presumably through strong interaction with the surface of SeNPs. The reaction of the sulfur group in glutathione peroxidase with selenium has been previously reported.^{28–31} Moreover, previous reports have shown that the presence of SH can stabilize selenium in the chemical environment.³² Thus, the formation of selenium–sulfur covalent binding between selenium nanoparticles and SH group of the peptide was likely. Mass spectroscopy data indicated the presence of S–Se in the fragment ion of cyclic peptide–S–Se (data were not shown). Thus, we assume that both covalent and noncovalent interactions are involved in the formation of peptide-capped selenium nanoparticles.

In addition to $[W_5R_4C]$ -SeNPs characterization, TEM microscopy was used to visualize the change on the size and morphology of nanoparticles after incubation with Dox. As shown in Figure 2, the shape of SeNPs was changed to multilayer ball-shape nanoparticles, suggesting the surface capping of SeNPs by peptides or interactions with Dox. The size range of nanoparticles was increased after incubation with Dox to 250–270 nm, showing a relatively significant change in

the diameter of nanoparticles due to entrapping or interaction with the drug. We speculate that Dox interacts with $[W_5R_4C]$ -SeNPs by covering the surface of peptide-capped SeNPs through intermolecular interactions (Figure 2). However, Dox (white cover) was not able to cover up the whole surface of the particles. The dark spots represent uncovered $[W_5R_4C]$ -SeNPs.

Circular Dichroism (CD). CD was used to determine whether the SeNPs formation can change the peptide secondary structure through intermolecular interactions. A comparative CD experiment was performed by using an aqueous solution of the peptide and its corresponding CP–SeNPs (50 μ M). CD spectra of $[W_5R_4C]$ showed a negative band at \sim 216 nm. Furthermore, a positive band was detected at \sim 230 nm. The CD spectra of $[W_5R_4C]$ -SeNPs showed a very similar CD pattern with a minimum peak at 216 nm. However, the maxima peak disappeared possibly because of the interaction of the peptide with SeNPs.

To determine whether $[W_5R_4C]$ -SeNPs can entrap marketed available drugs, CPT was used as a model drug in CD. CPT is a hydrophobic anticancer drug that works through inhibiting topoisomerase I activity.³³ The effect of CPT encapsulation by $[W_5R_4C]$ -SeNPs was investigated using CD to determine whether the secondary structure of the peptide changes in this process. As exhibited in Figure 3, $[W_5R_4C]$ -SeNP-loaded CPT demonstrated a significantly different CD pattern compared to that of CPT and $[W_5R_4C]$ -SeNPs alone. The results demonstrate that the interactions between the $[W_5R_4C]$ -SeNPs and CPT generates the new orientation of amino acids in the secondary structure, presumably through their involvement in the encapsulation process.

CPT's peak exhibited a maxima at 215 nm. The CD spectra of $[W_5R_4C]$ -SeNP-loaded CPT (5:1) showed a blue shift with a maxima at 209 nm, suggesting significant interaction of CPT with peptide-capped metal nanoparticles. These results were consistent with previously reported methods where conjugation and interaction of nanoparticles with their stabilizing ligands caused change in their CD pattern.^{23,24,34,35} Furthermore, change in CD patterns have been observed through an interaction between peptides and various types of drugs.³⁶

Encapsulation of Camptothecin by Peptide–SeNPs. Fluorescence spectroscopy was used to validate the entrapment

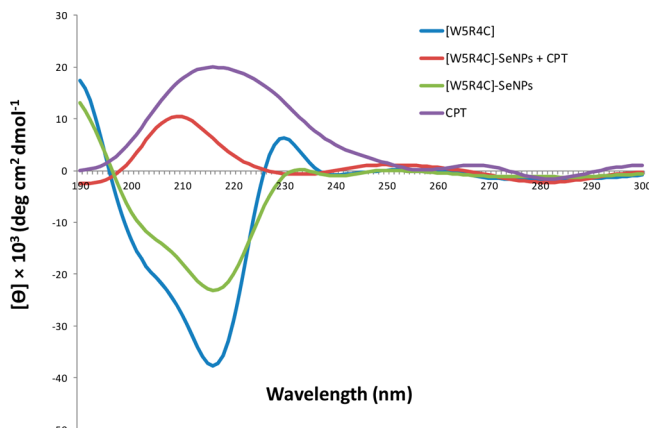


Figure 3. Comparative CD of cyclic $[\text{W}_5\text{R}_4\text{C}]$ and $[\text{W}_5\text{R}_4\text{C}]\text{-SeNPs}$ in the presence and absence of CPT.

of CPT by $[\text{W}_5\text{R}_4\text{C}]\text{-SeNPs}$. CPT is a hydrophobic anticancer drug that works through inhibiting topoisomerase I activity.³⁷ A significant blue shift in maxima's emission of CPT fluorescence spectra was found following the incubation of CPT by $[\text{W}_5\text{R}_4\text{C}]\text{-SeNPs}$. The characteristic CPT maximum peak at 442 nm was shifted to 431 nm after interaction of CPT with $[\text{W}_5\text{R}_4\text{C}]\text{-SeNPs}$ (Figure 4). The distribution of CPT in a

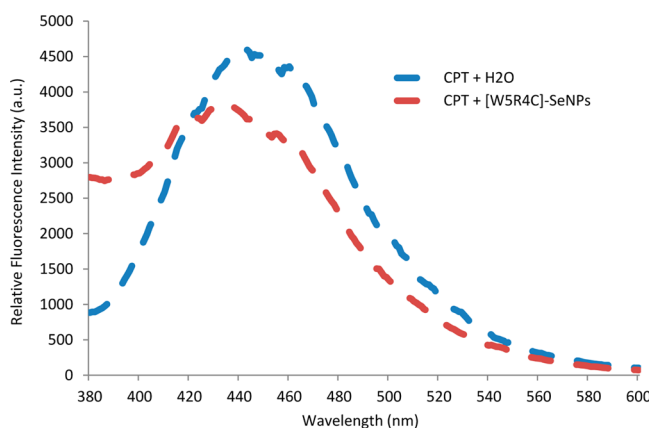


Figure 4. Fluorescence of CPT in the presence of $[\text{W}_5\text{R}_4\text{C}]\text{-SeNPs}$ (1:1 molar ratio) after 4 h of incubation. The assay was performed in triplicate ($n = 3$).

hydrophobic region and hydrophobic forces are possibly responsible for the observed blue shift of CPT's peak in the presence of $[\text{W}_5\text{R}_4\text{C}]\text{-SeNPs}$. Furthermore, the intensity of the peak was reduced presumably. We postulate that this is because of the self-quenching of bounded compound and the distribution and entrapment in the hydrophobic region formed by the CP-SeNPs.³⁸ The results are consistent with CD studies described above. These studies suggested that the cyclic peptide-SeNPs were capable of entrapment of CPT in the hydrophobic region possibly generated by involved tryptophans. We have previously reported the formation of hydrophobic regions through interactions of tryptophan residues.³⁹ Moreover, extended investigations showed that hydrophobic interactions occur between Dox and the self-assembled cyclic peptide.^{40,41} We assume that similar interactions occur between the cyclic peptide and CPT.

Drug Loading. Dox was chosen as a representative drug because of its high stability and inherent UV-vis properties to

investigate the quantity of the loaded drug by $[\text{W}_5\text{R}_4\text{C}]\text{-SeNPs}$. The loading efficiency experiment was conducted as described previously.⁴² Aqueous solution of Dox (100 μL of 200 μM) was mixed with the solution of $[\text{W}_5\text{R}_4\text{C}]\text{-SeNPs}$ in water (400 μL of 500 μM) to maintain a 1 to 10 molar ratio. After 24 h of incubation, the free Dox was collected by using the dialysis method.

The efficiency of $[\text{W}_5\text{R}_4\text{C}]\text{-SeNPs}$ to load Dox after 24 h was 45.6% when the ratio of Dox of $[\text{W}_5\text{R}_4\text{C}]\text{-SeNPs}$ by weight in feed was 1 to 10. Furthermore, loading capacity was found to be $16 \pm 1\%$ considering the weight ratio of Dox to $[\text{W}_5\text{R}_4\text{C}]\text{-SeNPs}$ (1:10) when the amount of SeNPs was determined using ICP-MS.

Cytotoxicity of Peptide-SeNPs. Fresh synthesized $[\text{W}_5\text{R}_4\text{C}]\text{-SeNPs}$ (50 μM) did not exhibit significant toxicity after 2 h in human ovarian adenocarcinoma (SK-OV-3), human leukemia (CCRF-CEM) cancer, and human embryonic kidney 293 (HEK-293T) cells. These data revealed that $[\text{W}_5\text{R}_4\text{C}]\text{-SeNPs}$ (50 μM) has minimal toxicity (8–10%) in SK-OV-3, CCRF-CEM, and HEK-293T cells (Figure 5). Therefore, $[\text{W}_5\text{R}_4\text{C}]\text{-SeNPs}$ concentration was maintained at 50 μM for further flow cytometry studies.

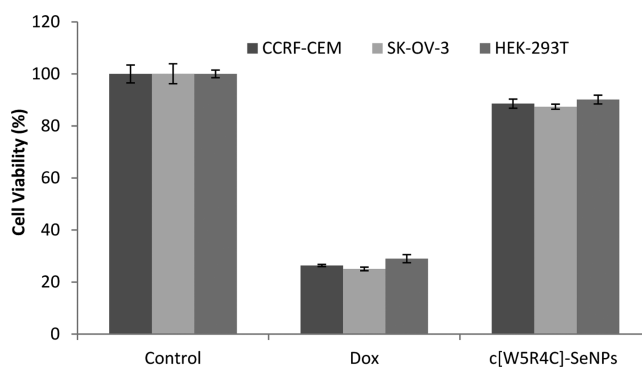


Figure 5. Cytotoxicity of the cyclic peptide and corresponding CP-SeNPs. The assay was performed in triplicate ($n = 3$).

Evaluation of Peptide-SeNPs as Molecular Transporters. $[\text{WR}]_4$ cyclic structure contributes significantly to its cell-penetrating ability.²² To determine whether CP-SeNPs can act as drug carriers, a clinically used anticancer drug, dasatinib (Das), was employed as a cargo molecule. Dasatinib is a nonselective tyrosine kinase inhibitor against Src, Abl, and BCR. Dasatinib is used clinically for the treatment of Philadelphia chromosome-positive acute lymphoblastic leukemia (Ph⁺ ALL) and chronic myeloid leukemia (CML).⁴³ To detect the transportation of the drug by CP-SeNPs for cell-based studies, we synthesized a carboxyfluorescein conjugate of Das (F'-Das). Then the incubation of CCRF-CEM cells and F'-Das (5 μM) was conducted for 2 h with or without diluted $[\text{W}_5\text{R}_4\text{C}]\text{-SeNPs}$ (50 μM) and the corresponding parent peptide $[\text{W}_5\text{R}_4\text{C}]$ (50 μM).

After 2 h, the cell surface-attached fluorescence-labeled drug was washed with trypsin. F'-Das (5 μM) intracellular uptake was evaluated by a flow cytometry technique. Flow cytometry results indicated that cells incubated with F'-drug mixed with $[\text{W}_5\text{R}_4\text{C}]\text{-SeNPs}$ and F'-drug mixed with $[\text{W}_5\text{R}_4\text{C}]$ (50 μM) have notably higher fluorescence intensity compared to that in cells incubated with F'-Das alone. $[\text{W}_5\text{R}_4\text{C}]\text{-SeNPs}$ and $[\text{W}_5\text{R}_4\text{C}]$ improved the intracellular uptake of F'-Das by 9.5-

and 4.3-folds when compared with the cells treated with F'-Das alone (Figure 6).

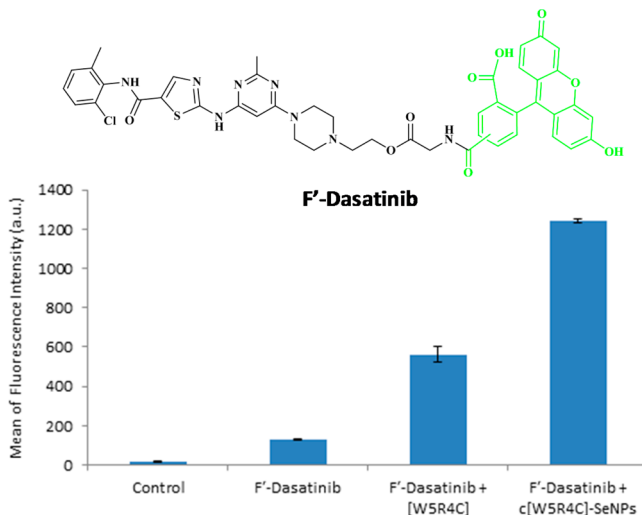


Figure 6. Uptake of F'-Das with $[W_5R_4C]$ and $[W_5R_4C]$ -SeNPs by cells after 2 h. The assay was performed in triplicate ($n = 3$).

Furthermore, flow cytometry results demonstrated that the cellular uptake of the fluorescently labeled drug was improved by 2.2-fold with peptide-capped SeNPs compared to that with the peptide. The data reveal that both the peptide and SeNPs in $[W_5R_4C]$ -SeNPs contribute to the improvement of the cellular uptake of the drug in a higher degree. The enhancement of cellular delivery of F'-Das with $[W_5R_4C]$ and $[W_5R_4C]$ -SeNPs indicates that the peptide alone has the potential to work as a drug carrier. However, the transporting efficiency of the peptide was enhanced after interaction with SeNPs presumably due to a change in the peptide secondary structure leading to higher efficiency in drug entrapment. These data correlate well with CD results that were described above.

Confocal microscopy was employed to visualize the enhancement of F'-Das ($5 \mu\text{M}$) uptake by SKOV-3 cells. No fluorescence intensity was observed in treated cells with F'-Das alone. However, high fluorescence intracellular intensity was observed in the presence of F'-Das-loaded $[W_5R_4C]$ -SeNPs ($50 \mu\text{M}$) when compared with that of drug after 2 h (Figure 7). We used DAPI to mark the nucleus of cells. Confocal

microscopy images displayed that F'-Das was mostly localized in the nucleus of SK-OV-3 cells when mixed with $[W_5R_4C]$ -SeNPs after 2 h incubation.

After evaluating $[W_5R_4C]$ -SeNPs as a molecular transporter of a small-molecule drug, its potential was examined for transporting a relatively large negatively charged phosphopeptide with limited cellular permeability. Having negatively charged phosphate groups and relatively large size of phosphopeptides make their intracellular delivery a challenging task. Here, a model phosphopeptide, PEPYLGLD, was used for further studies. The sequence of amino acid in PEPYLGLD mimics the phosphotyrosine 1246 of ErbB2 that binds to the Chk SH2 domain.⁴⁴ CP-SeNPs were examined for the cellular delivery of fluorescence conjugate of PEPYLGLD (F'-PEPYLGLD) using CCRF-CEM cells. The synthesis of F'-PEPYLGLD has been previously described by us.⁴⁵ The analysis of flow cytometry results showed that the F'-PEPYLGLD ($5 \mu\text{M}$) uptake was improved by 25-fold when mixed with $[W_5R_4C]$ -SeNPs ($50 \mu\text{M}$) compared to that of F'-PEPYLGLD alone, suggesting that $[W_5R_4C]$ -SeNPs may work as a F'-PEPYLGLD carrier. $[W_5R_4C]$ -SeNPs increased the F'-PEPYLGLD uptake by 1.4-fold when compared to that of $[W_5R_4C]$ (Figure 8). These data propose that SeNPs have a significant effect on enhancing the cellular uptake of the phosphopeptide.

The intracellular uptake enhancement of F'-PEPYLGLD by $[W_5R_4C]$ -SeNPs was also confirmed via confocal microscopy. A comparative microscopy investigation was performed by comparing F'-PEPYLGLD ($5 \mu\text{M}$)-loaded $[W_5R_4C]$ -SeNP ($50 \mu\text{M}$) fluorescence intensity with that of F'-PEPYLGLD ($5 \mu\text{M}$) alone in SK-OV-3 cells. The cells were incubated with treatments for 2 h at 37°C . No green fluorescence was seen in cells when they were incubated with F'-PEPYLGLD alone. This part of our findings suggests that the phosphopeptide alone could not cross the cellular membrane. However, when $[W_5R_4C]$ -SeNPs were used, a significantly higher fluorescence intensity was observed, showing that CP-SeNPs can work as a transporter system for the fluorescein-labeled phosphopeptide. Merged images revealed that the phosphopeptide in combination with peptide-SeNPs was mostly localized in the nuclei of SK-OV-3 cells (Figure 9). The imaging results showed that $[W_5R_4C]$ -SeNPs presence is critical to increase the cellular delivery of the cell impermeable phosphopeptide.

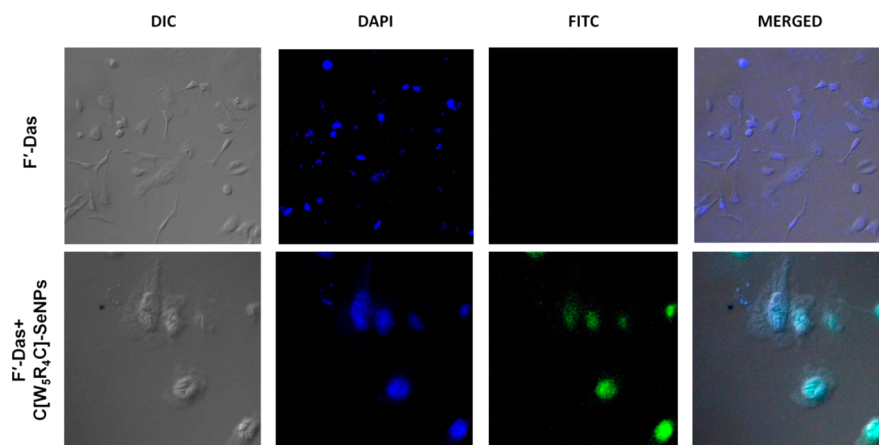


Figure 7. Images of the cellular uptake of F'-Das in SK-OV-3 cells with or without $[W_5R_4C]$ -SeNPs after 2 h of incubation.

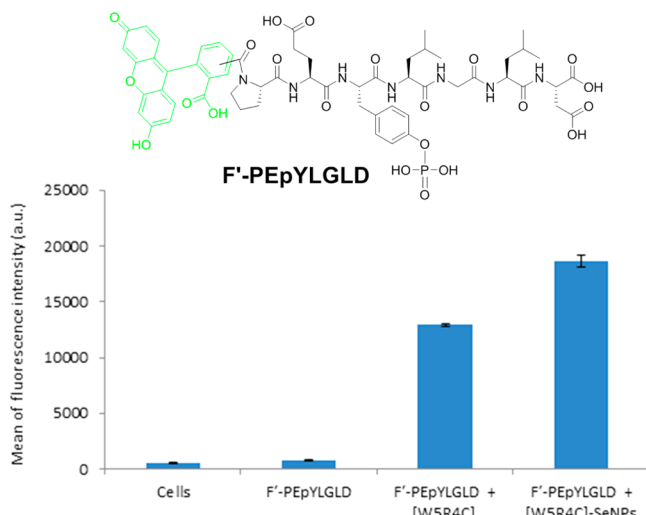


Figure 8. F'-PEpYLGLD uptake by cells when used in combination with $[W_5R_4C]$ -SeNPs and $[W_5R_4C]$ after 2 h of incubation. The assay was performed in triplicate ($n = 3$).

Mechanistic Studies of Cellular Internalization. Molecular cargos can employ various mechanisms for cellular entry. These mechanisms include micropinocytosis, phagocytosis, and receptor-mediated endocytosis (RME) pathways. Caveolae-mediated, clathrin-mediated, and clathrin/caveolae independent endocytosis are examples of RME.⁴⁶ To investigate possible transportation mechanism of CP-SeNPs cellular uptake, the fluorescence intensity of F'-PEpYLGLD loaded $[W_5R_4C]$ -SeNPs (1:10) was quantified in combination with several endocytic inhibitors like nystatin, chloroquine, chlorpromazine, 5-(*N*-ethyl-*N*-isopropyl)-amiloride (EIA), and methyl- β -cyclodextrin by using flow cytometry.

Figure 10 shows the uptake of F'-PEpYLGLD loaded $[W_5R_4C]$ -SeNPs by cells did not significantly decrease in the presence of chloroquine, chlorpromazine, and methyl- β -cyclodextrin after 2 h incubation at 37 °C in SK-OV-3 cells. These data suggest that clathrin-mediated or caveolae-mediated

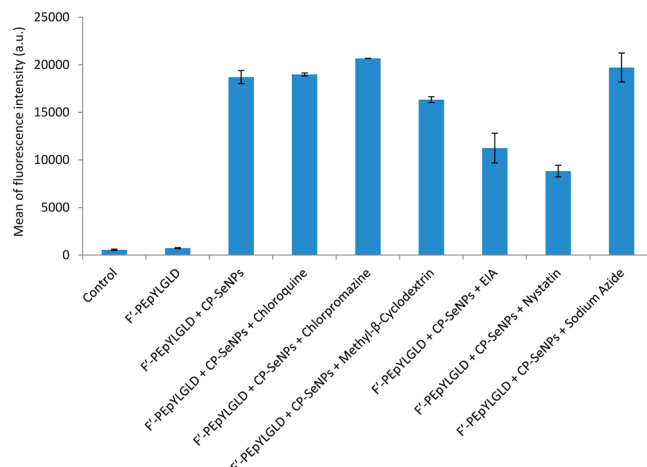


Figure 10. Flow cytometry showing the uptake of F'-PEpYLGLD loaded $[W_5R_4C]$ -SeNPs with or without various endocytic inhibitors in SK-OV-3 cells after 2 h. The assay was performed in triplicate ($n = 3$).

endocytosis and phagocytosis are not the only mechanisms of cellular uptake.^{47–49} However, the uptake of the cargo molecule was inhibited by 52% and 40% when nystatin and EIA were used, respectively, showing that caveolae-mediated and macropinocytosis pathways could be two of the involved mechanisms for the internalization of cargo molecules by functionalized SeNPs. Moreover, as it is evident in Figure 10, these two inhibitors did not block the uptake of cargo completely, meaning that other endocytic pathways are also involved in the delivery of F'-PEpYLGLD-loaded $[W_5R_4C]$ -SeNPs. In addition to endocytic inhibitors, sodium azide was employed as an ATP depleting agent. The results revealed that F'-PEpYLGLD uptake did not alter in combination with sodium azide showing that ATP depletion is not involved in the mechanism of uptake.

The surface functionalization of SeNPs by using the peptide could improve the primary interactions of involved amino acids, such as tryptophan and arginine, with the lipid bilayer's

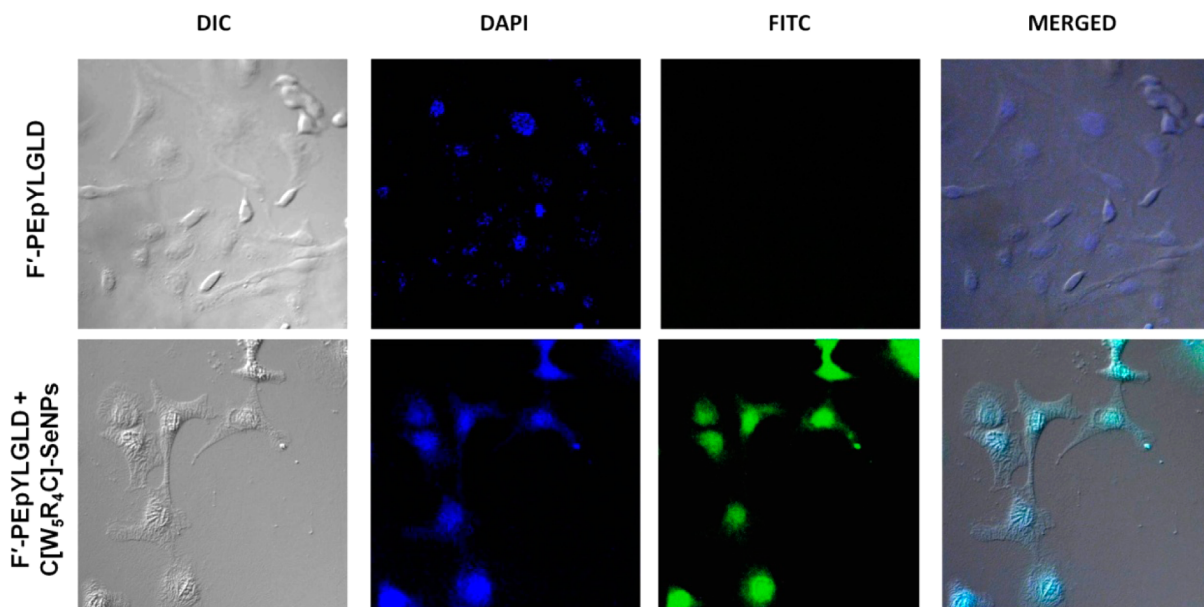


Figure 9. Microscopy images of F'-PEpYLGLD with and without $[W_5R_4C]$ -SeNPs in SK-OV-3 cells after 2 h.

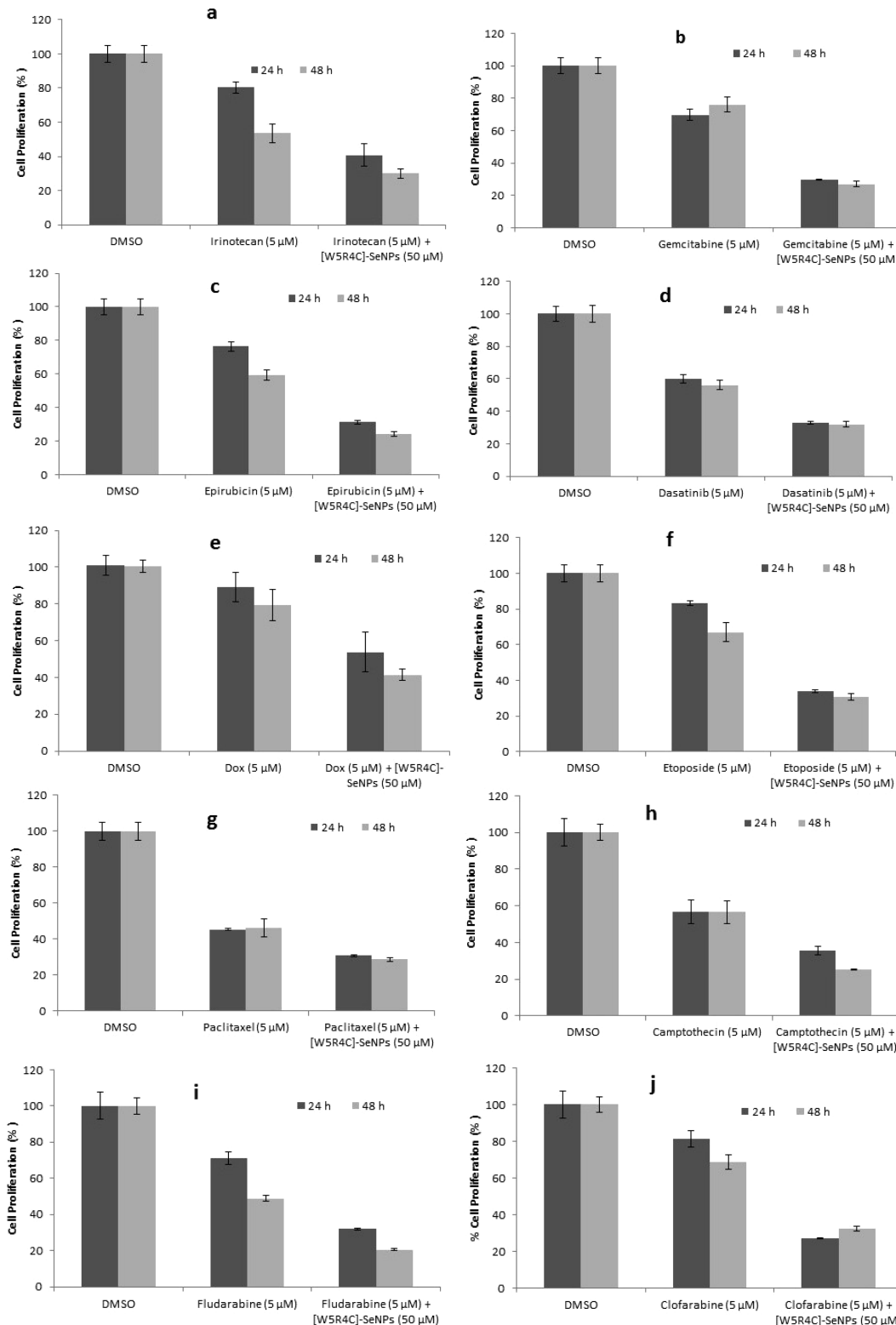


Figure 11. Time-dependent antiproliferative assay of (a) irinotecan, (b) gemcitabine, (c) epirubicin, (d) dasatinib, (e) doxorubicin, (f) etoposide, (g) paclitaxel, (h) camptothecin, (i) fludarabine, and (j) clofarabine in the absence and presence of $[W_5R_4C]$ -SeNPs. The experiments were conducted in triplicate ($n = 3$).

hydrophobic groups and negatively charged phospholipids present in the cell membrane. This electrostatic/hydrophobic interactions could trigger the complex to cross the phospholipid bilayer. Tryptophan residues can generate hydrophobic forces, disturb the available phospholipids, and

cause distortion of the exterior phospholipid monolayer. Subsequently, peptide internalizes into the membrane and improves the cargo cellular entry. The surface decoration of SeNPs by the peptide structure can improve nanoparticle stability and influence the cellular uptake mechanism. However,

to get a detailed understanding of the uptake mechanism by these CP–SeNPs, further investigations are required.

Intracellular Delivery of Dox. To explore the drug cellular release profile by the carrier, Dox was employed as a representative drug. A HPLC technique was used to investigate the intracellular release of Dox by $[W_5R_4C]$ –SeNPs–Dox complex in CCRF–CEM cells. CCRF–CEM cells (1.2×10^7) were incubated with $[W_5R_4C]$ –SeNPs (50 μM) loaded with Dox (5 μM) for various times (12–48 h). The quantity of the released Dox was calculated by analyzing HPLC data at 490 nm after different time intervals. The data showed that $[W_5R_4C]$ –SeNPs–Dox releases Dox following a time-dependent pattern. The HPLC profile showed that Dox appeared in a retention time of 15.8–15.9 min (Figure S2, Supporting Information). HPLC results exhibited that, after 12, 24, and 48 h of incubation in cells, 10.5, 20, and 40% of Dox was released, respectively. The HPLC profile showed that a sustained/slow release of Dox play an important role in the overall activity of the $[W_5R_4C]$ –SeNPs loaded with Dox as a potential prodrug.

Antiproliferative Assay Studies. The antiproliferative activity of several anticancer drugs including Dox, gemcitabine, clofarabine, etoposide, camptothecin, irinotecan, epirubicin, fludarabine, dasatinib, and paclitaxel were examined in SK-OV-3 cells with and without $[W_5R_4C]$ –SeNPs in a time-dependent pattern. The experiments were used to investigate the impact of using $[W_5R_4C]$ –SeNPs in the biological doses of anticancer drugs in cells.

The antiproliferative results revealed that the activity of all anticancer drugs (5 μM), Dox, gemcitabine, clofarabine, etoposide, camptothecin, irinotecan, epirubicin, fludarabine, dasatinib, and paclitaxel was enhanced when combined with $[W_5R_4C]$ –SeNPs (50 μM) after 48 h in SK-OV-3 cells by 38%, 49%, 36%, 36%, 31%, 30%, 30%, 28%, 24%, and 17%, respectively. This effect could be due to improving the cellular uptake of the drugs (Figure 11). In addition, the degradation of peptide-capped SeNPs complex could generate aggregated toxic selenium leading to the synergistic effect in cancer cells. The antiproliferative results showed the sustained release of drugs in cells in a time-dependent pattern in SK-OV-3 cells.

CONCLUSIONS

A novel group of DDSs was synthesized from SeNPs and cell-penetrating peptide having tryptophan, arginine, and cysteine residues. $[W_5R_4C]$ –SeNPs showed an ability to interact with CPT, a hydrophobic drug, possibly via noncovalent forces. This system transported a fluorescence conjugate of labeled dasatinib and a negatively charged cell-impermeable phosphopeptide (F'-PEpYLGLD) into cells. Confocal microscopy showed that $[W_5R_4C]$ –SeNPs delivered cargos intracellularly. The antiproliferative activities of several anticancer drugs, such as doxorubicin, gemcitabine, clofarabine, etoposide, camptothecin, irinotecan, epirubicin, fludarabine, dasatinib, and paclitaxel, were significantly enhanced in the presence of $[W_5R_4C]$ –SeNPs. This work provides insights for the design of peptide–metal nanoparticle novel drug delivery systems.

ASSOCIATED CONTENT

Supporting Information

Synthesis of fluorescence-labeled dasatinib, analytical HPLC, and release profile of Dox. This material is available free of charge via the Internet at <http://pubs.acs.org>.

AUTHOR INFORMATION

Corresponding Author

*(K.P.) Tel: +1-714-516-5489. Fax: +1-714-516-5481. E-mail: parang@chapman.edu.

Present Address

||(Y.A.B.) Department of Chemistry, Tennessee State University, Nashville, TN 37209, United States

Notes

The authors declare no competing financial interest.

ACKNOWLEDGMENTS

We thank National Center for Research Resources, NIH (Grant No. 8 P20 GM103430-12), for sponsoring the core facility.

REFERENCES

- (1) Zhang, Y.; Chan, H. F.; Leong, K. W. Advanced materials and processing for drug delivery: The past and the future. *Adv. Drug Delivery Rev.* **2013**, *65*, 104–120.
- (2) Andrade, F.; Rafael, D.; Videira, M.; Ferreira, D.; Sosnik, A.; Sarmento, B. Nanotechnology and pulmonary delivery to overcome resistance in infectious diseases. *Adv. Drug Delivery Rev.* **2013**, *65*, 1816–1827.
- (3) Mei, L.; Zhang, Z.; Zhao, L.; Huang, L.; Yang, X.-L.; Tang, J.; Feng, S.-S. Pharmaceutical nanotechnology for oral delivery of anticancer drugs. *Adv. Drug Delivery Rev.* **2013**, *65*, 880–890.
- (4) Swami, A.; Shi, J.; Gadde, S.; Votruba, A. R.; Kolishetti, N.; Farokhzad, O. C. Nanoparticles for Targeted and Temporally Controlled Drug Delivery. In *Multifunctional Nanoparticles for Drug Delivery Applications*; Springer: New York, 2012; pp 9–29.
- (5) Ahmad, M. Z.; Akhter, S.; Jain, G. K.; Rahman, M.; Pathan, S. A.; Ahmad, F. J.; Khar, R. K. Metallic nanoparticles: technology overview & drug delivery applications in oncology. *Expert Opin. Drug Delivery* **2010**, *7*, 927–942.
- (6) Vekariya, K.; Kaur, J.; Tikoo, K. Signaling imparts chemotherapeutic selectivity to selenium nanoparticles in breast cancer. *Nanomed.: Nanotechnol., Biol. Med.* **2012**, *8*, 1125–1132.
- (7) Yang, G.; Zhou, R. Further observations on the human maximum safe dietary selenium intake in a seleniferous area of China. *J. Trace Elem. Electrolytes Health Dis.* **1994**, *8*, 159.
- (8) Sarin, L.; Sanchez, V. C.; Yan, A.; Kane, A. B.; Hurt, R. H. Selenium–carbon bifunctional nanoparticles for the treatment of malignant mesothelioma. *Adv. Mater.* **2010**, *22*, 5207–5211.
- (9) Wang, D.; Taylor, E. W.; Wang, Y.; Wan, X.; Zhang, J. Encapsulated nanoepigallocatechin-3-gallate and elemental selenium nanoparticles as paradigms for nanochemoprevention. *Int. J. Nanomed.* **2012**, *7*, 1711–21.
- (10) Gliga, A. R.; Skoglund, S.; Wallinder, I. O.; Fadeel, B.; Karlsson, H. L. Size-dependent cytotoxicity of silver nanoparticles in human lung cells: the role of cellular uptake, agglomeration and Ag release. *Part. Fibre Toxicol.* **2014**, *11*, 11.
- (11) Zhu, J.; Liao, L.; Zhu, L.; Zhang, P.; Guo, K.; Kong, J.; Ji, C.; Liu, B. Size-dependent cellular uptake efficiency, mechanism, and cytotoxicity of silica nanoparticles toward HeLa cells. *Talanta* **2013**, *107*, 408–415.
- (12) Liu, W.; Li, X.; Wong, Y.-S.; Zheng, W.; Zhang, Y.; Cao, W.; Chen, T. Selenium nanoparticles as a carrier of 5-fluorouracil to achieve anticancer synergism. *ACS Nano* **2012**, *6*, 6578–6591.
- (13) Zhang, Y.; Li, X.; Huang, Z.; Zheng, W.; Fan, C.; Chen, T. Enhancement of cell permeabilization apoptosis-inducing activity of selenium nanoparticles by ATP surface decoration. *Nanomed.: Nanotechnol., Biol. Med.* **2012**, *9*, 74–84.
- (14) Yang, F.; Tang, Q.; Zhong, X.; Bai, Y.; Chen, T.; Zhang, Y.; Li, Y.; Zheng, W. Surface decoration by *Spirulina* polysaccharide enhances the cellular uptake and anticancer efficacy of selenium nanoparticles. *Int. J. Nanomed.* **2012**, *7*, 835–844.

- (15) Wu, H.; Li, X.; Liu, W.; Chen, T.; Li, Y.; Zheng, Y.; Man, C. W.-M.; Wong, M.-K.; Wong, K.-H. Surface decoration of selenium nanoparticles by mushroom polysaccharides–protein complexes to achieve enhanced cellular uptake and antiproliferative activity. *J. Mater. Chem.* **2012**, *22*, 9602–9610.
- (16) Yu, B.; Zhang, Y.; Zheng, W.; Chen, T. Positive surface charge enhances selective cellular uptake and anticancer efficacy of selenium nanoparticles. *Inorg. Chem.* **2012**, *51*, 8956–8963.
- (17) Langel, U. *Cell-Penetrating Peptides: Processes and Applications*; CRC Press: Boca Raton, FL, 2002.
- (18) Torchilin, V. P.; Rammohan, R.; Weissig, V.; Levchenko, T. S. TAT peptide on the surface of liposomes affords their efficient intracellular delivery even at low temperature and in the presence of metabolic inhibitors. *Proc. Natl. Acad. Sci. U.S.A.* **2001**, *98*, 8786–8791.
- (19) Silhol, M.; Tyagi, M.; Giacca, M.; Lebleu, B.; Vives, E. Different mechanisms for cellular internalization of the HIV-1 Tat-derived cell penetrating peptide and recombinant proteins fused to Tat. *Eur. J. Biochem.* **2002**, *269*, 494–501.
- (20) Thorn, P. E.; Persson, D.; Isakson, P.; Goksör, M.; Onfelt, A.; Nordén, B. Uptake of analogs of penetratin, Tat(48–60) and oligoarginine in live cells. *Biochem. Biophys. Res. Commun.* **2003**, *307*, 100–107.
- (21) Kim, C. K.; Ghosh, P.; Pagliuca, C.; Zhu, Z.-J.; Menichetti, S.; Rotello, V. M. Entrapment of hydrophobic drugs in nanoparticle monolayers with efficient release into cancer cells. *J. Am. Chem. Soc.* **2009**, *131*, 1360–1361.
- (22) Mandal, D.; Nasrolahi Shirazi, A.; Parang, K. Cell-penetrating homochiral cyclic peptides as nuclear-targeting molecular transporters. *Angew. Chem., Int. Ed.* **2011**, *50*, 9633–9637.
- (23) Nasrolahi Shirazi, A.; Mandal, D.; Tiwari, R.; Guo, L.; Lu, W.; Parang, K. Cyclic peptide-capped gold nanoparticles as drug delivery systems. *Mol. Pharmacol.* **2012**, *10*, 500–511.
- (24) Oh, D.; Darwish, S. A.; Shirazi, A. N.; Tiwari, R. K.; Parang, K. Amphiphilic bicyclic peptides as cellular delivery agents. *ChemMed. Chem.* **2014**, DOI: 10.1002/cmde.201402230.
- (25) Nasrolahi Shirazi, A.; Tiwari, R. K.; Brown, A.; Mandal, D.; Sun, G.; Parang, K. Cyclic peptides containing tryptophan and arginine as Src kinase inhibitors. *Bioorg. Med. Chem. Lett.* **2013**, *23*, 3230–3234.
- (26) Nasrolahi Shirazi, A.; Tiwari, R. K.; Chhikara, B. S.; Mandal, D.; Parang, K. Design and biological evaluation of cell-penetrating peptide–doxorubicin conjugates as prodrugs. *Mol. Pharmaceutics* **2013**, *10*, 488–499.
- (27) Tan, Y. N.; Lee, J. Y.; Wang, D. I. C. Uncovering the design rules for peptide synthesis of metal nanoparticles. *J. Am. Chem. Soc.* **2010**, *132*, 5677–5686.
- (28) Baker, R. D.; Baker, S. S.; Larosa, K.; Whitney, C.; Newburger, P. E. Selenium regulation of glutathione peroxidase in human hepatoma cell line Hep3B. *Arch. Biochem. Biophys.* **1993**, *304*, 53–57.
- (29) Siddons, R. C.; Mills, C. F. Glutathione peroxidase activity and erythrocyte stability in calves differing in selenium and vitamin E status. *Br. J. Nutr.* **1981**, *46*, 345–355.
- (30) Li, S.; Shen, Y.; Xie, A.; Yu, X.; Zhang, X.; Yang, L.; Li, C. Rapid, room-temperature synthesis of amorphous selenium/protein composites using *Capsicum annuum* L extract. *Nanotechnology* **2007**, *18*, 405101–9.
- (31) Chen, Z.; Shen, Y.; Xie, A.; Zhu, J.; Wu, Z.; Huang, F. L-Cysteine-assisted controlled synthesis of selenium nanospheres and nanorods. *Cryst. Growth Des.* **2009**, *9*, 1327–1333.
- (32) Bermano, G.; Arthur, J. R.; Hesketh, J. E. Selective control of cytosolic glutathione peroxidase and phospholipid hydroperoxide glutathione peroxidase mRNA stability by selenium supply. *FEBS Lett.* **1996**, *387*, 157–160.
- (33) Garcia-Carbonero, R.; Supko, J. G. Current perspectives on the clinical experience, pharmacology, and continued development of the camptothecins. *Cancer Res.* **2002**, *8*, 641–661.
- (34) Slocik, J. M.; Govorov, A. O.; Naik, R. R. Plasmonic circular dichroism of peptide-functionalized gold nanoparticles. *Nano Lett.* **2011**, *11*, 701–705.
- (35) Petkova, G. A.; Záruba, K.; Žvátorová, P.; Králík, V. Gold and silver nanoparticles for biomolecule immobilization and enzymatic catalysis. *Nanoscale Res. Lett.* **2012**, *7*, 287–297.
- (36) Reid, R. E.; Cariepy, J.; Hodges, R. S. Interaction of neuroleptic drugs with a synthetic calcium-binding peptide analog of site III of rabbit skeletal troponin C. Phenothiazine selective binding. *FEBS Lett.* **1983**, *154*, 60–64.
- (37) Garcia-Carbonero, R.; Supko, J. G. Current perspectives on the clinical experience, pharmacology, and continued development of the camptothecins. *Cancer Res.* **2002**, *8*, 641–661.
- (38) Kailasan, A.; Yuan, Q.; Yang, H. Synthesis and characterization of thermoresponsive polyamidoamine-polyethylene glycol-poly(D,L-lactide) core-shell nanoparticles. *Acta Biomater.* **2009**, *6*, 1131–1139.
- (39) Mandal, D.; Tiwari, R. K.; Nasrolahi Shirazi, A.; Oh, D.; Ye, G.; Banerjee, A.; Yadav, A.; Parang, K. Self-assembled surfactant cyclic peptide nanostructures as stabilizing agents. *Soft Matter* **2013**, *9*, 9465–9475.
- (40) Nasrolahi Shirazi, A.; Tiwari, R. K.; Oh, D.; Sullivan, B.; McCaffrey, K.; Mandal, D.; Parang, K. Surface decorated gold nanoparticles by linear and cyclic peptides as molecular transporters. *Mol. Pharmaceutics* **2013**, *10*, 3137–3151.
- (41) Mandal, D.; Nasrolahi Shirazi, A.; Parang, K. Self-assembly of peptides to nanostructures. *Org. Biomol. Chem.* **2014**, *12*, 3544–3561.
- (42) Nasrolahi Shirazi, A.; Oh, D.; Tiwari, R. K.; Sullivan, B.; Gupta, A.; Bothun, G. D.; Parang, K. Peptide-amphiphile containing arginine and fatty acyl chains as molecular transporters. *Mol. Pharmaceutics* **2013**, *10*, 4717–4727.
- (43) Harbaum, L.; Marx, A.; Goekkurt, E.; Schafhausen, P.; Atanackovic, D. Treatment with dasatinib for chronic myeloid leukemia following imatinib-induced hepatotoxicity. *Int. J. Hematol.* **2013**, *99*, 91–94.
- (44) Machida, K.; Mayer, B. J. The SH2 domain: versatile signaling module and pharmaceutical target. *Biochim. Biophys. Acta* **2005**, *1747*, 1–25.
- (45) Nasrolahi Shirazi, A.; Tiwari, R. K.; Oh, D.; Banerjee, A.; Yadav, A.; Parang, K. Efficient delivery of cell impermeable phosphopeptides by a cyclic peptide amphiphile containing tryptophan and arginine. *Mol. Pharmaceutics* **2013**, *10*, 2008–2020.
- (46) Conner, S. D.; Schmid, S. L. Regulated portals of entry into the cell. *Nature* **2003**, *422*, 37–44.
- (47) Chen, C.-L.; Hou, W. H.; Liu, I. H.; Hsiao, G.; Huang, S. S.; Huang, J. S. Inhibitors of clathrin-dependent endocytosis enhance TGFbeta signaling and responses. *J. Cell. Sci.* **2009**, *122*, 1863–1871.
- (48) Hussain, K. M.; Leong, K. L.; Ng, M. M.; Chu, J. J. The essential role of clathrin-mediated endocytosis in the infectious entry of human enterovirus 71. *J. Biol. Chem.* **2011**, *286*, 309–21.
- (49) Oh, D.; Nasrolahi Shirazi, A.; Northup, K.; Sullivan, B.; Tiwari, R. K.; Bisoffi, M.; Parang, K. Enhanced cellular uptake of short polyarginine peptides through fatty acylation and cyclization. *Mol. Pharmaceutics* **2014**, *11*, 2845–2854.